

Universal critical behavior of the two-magnon-bound-state mass gap for the (2 + 1)-dimensional Ising model

Yoshihiro Nishiyama

*Department of Physics, Faculty of Science, Okayama University, Okayama 700-8530,
Japan*

Abstract

The two-magnon-bound-state mass gap m_2 for the two-dimensional quantum Ising model was investigated by means of the numerical diagonalization method; the low-lying spectrum is directly accessible via the numerical diagonalization method. It has been claimed that the ratio m_2/m_1 (m_1 : one-magnon mass gap) is a universal constant in the vicinity of the critical point. Aiming to suppress corrections to scaling (lattice artifact), we consider the spin- $S = 1$ Ising model with finely-adjusted extended interactions. The simulation result for the finite-size cluster with $N \leq 20$ spins indicates the mass-gap ratio $m_2/m_1 = 1.84(1)$.

Keywords:

05.50.+q 05.10.-a 05.70.Jk 64.60.-i

1. Introduction

The magnons of the Ising ferromagnet in the symmetry-broken phase are attractive, forming a bound state with a mass gap $m_2 (< 2m_1)$ (m_1 : one-magnon mass gap) [1, 2, 3, 4, 5, 6, 7, 8, 9, 10, 11, 12]. Recently, such a bound state was observed [13] for a quasi-one-dimensional quantum Ising ferromagnet, CoNb_2O_6 , by means of the inelastic neutron scattering. A notable point is that the mass-gap ratio m_2/m_1 approaches to a constant value, namely, $m_2/m_1 \rightarrow (1 + \sqrt{5})/2$ (golden ratio), asymptotically in the vicinity of the critical point (between the ferromagnetic and paramagnetic phases). As a matter of fact, according to the field-theoretical rigorous analysis [1, 2], the mass-gap ratio m_2/m_1 is a universal constant (golden ratio) at the critical

point, providing a novel type of the critical amplitude relation; see Ref. [3] for a review. It would be intriguing that the spectral property is also under the reign of universality.

On the contrary, no rigorous information is available as to the two- (three-) dimensional quantum (classical) Ising model, and a variety of approaches have been made to clarify the nature of the two-magnon bound state [4, 5, 6, 7, 8, 9, 10, 11, 12]; afterward, we make an overview. The aim of this paper is to calculate the mass-gap ratio m_2/m_1 for the two-dimensional spin- $S = 1$ transverse-field (quantum) Ising model [14] by means of the numerical diagonalization method; technical details are explained in Sec. 2. As mentioned above, the spin magnitude is extended to $S = 1$ from $S = 1/2$ [14]. The spin- $S = 1$ model allows us to incorporate a variety of interactions, with which corrections to scaling (lattice artifact) are suppressed considerably; see Ref. [15], and references therein.

We make an overview of the the preceding studies. By means of the Monte Carlo method for the three-dimensional lattice- ϕ^4 and Ising models up to $60^2 \cdot 120$ sites, the mass-gap ratio was estimated as $m_2/m_1 = 1.83(3)$ [4]. Here, the reciprocal correlation length $1/\xi$ was identified as the mass gap. The result was supported by a perturbative analysis of the three-dimensional ϕ^4 field theory, $m_2/m_1 = 1.828(3)$ [10]; the next-leading-order result, however, leads to an unphysical conclusion $m_2/m_1 < 0$, indicating a highly non-perturbative nature of this issue. The transfer-matrix (TM) simulation for the three-dimensional classical Ising model with $N \leq 15$ spins (N : number of spins constituting a TM slice) indicates $m_2/m_1 = 1.84(3)$ [11]. A recent cluster-expansion analysis of the two-dimensional transverse-field Ising model yields an estimate $m_2/m_1 \approx 1.81$ [12] through a careful resummation of the power series.

As mentioned above, we consider the two-dimensional spin- $S = 1$ transverse-field Ising model (1). The motivation of this paper is twofold. First, we treat a larger cluster with $N \leq 20$ spins, taking an advantage in that the Hamiltonian matrix has few non-zero elements; note that a cluster with $N \leq 15$ spins was simulated [11] with the transfer-matrix method (for the three-dimensional classical Ising model), where the matrix is not sparse, and computationally demanding. Second, the extension of the spin magnitude from $S = 1/2$ to $S = 1$ allows us to incorporate a variety of interactions such as the single-ion anisotropy D , and the biquadratic exchange interactions (J_4, J'_4); see Eq. (1). As mentioned afterward, those coupling constants are finely adjusted [14] so as to eliminate corrections to scaling, namely, the lattice

artifact; actually, the subsequent finite-size-scaling analysis of criticality is improved significantly by the finely-adjusted coupling constants [14]. A recent extensive Monte Carlo simulation for the $S = 1$ Ising model is reported in Ref. [15].

To be specific, the Hamiltonian for the two-dimensional spin- $S = 1$ transverse-field Ising model [14] is given by

$$\begin{aligned} \mathcal{H} = & -J \sum_{\langle ij \rangle} S_i^z S_j^z - J' \sum_{\langle\langle ij \rangle\rangle} S_i^z S_j^z - J_4 \sum_{\langle ij \rangle} (S_i^z S_j^z)^2 \\ & - J'_4 \sum_{\langle\langle ij \rangle\rangle} (S_i^z S_j^z)^2 + D \sum_i (S_i^z)^2 - \Gamma \sum_i S_i^x - H \sum_i S_i^z. \end{aligned} \quad (1)$$

Here, the quantum $S = 1$ operators $\{\mathbf{S}_i\}$ are placed at each square-lattice point i ($i = 1, 2, \dots, N$). The summations, $\sum_{\langle ij \rangle}$ and $\sum_{\langle\langle ij \rangle\rangle}$, run over all possible nearest-neighbor and next-nearest-neighbor pairs, respectively. The parameters J and J' are the corresponding coupling constants. (As mentioned above, the interaction parameters, D , J_4 , and J'_4 , denote the single-ion-anisotropy, biquadratic-nearest-neighbor, and biquadratic-next-nearest-neighbor coupling constants, respectively.) The parameters Γ and H are the transverse and longitudinal magnetic fields, respectively. According to Ref. [14], a critical point locates at

$$(J, J', J_4, J'_4, D, \Gamma, H) = [0.41191697085, 0.16125069616, -0.11764020018, -0.05267926601, -0.39781956122, 1.0007(17), \mathbf{(2)}]$$

where corrections to scaling (lattice artifact) are suppressed considerably. The set of coupling constants, Eq. (2), were determined through two-step procedures. First, with $\Gamma = 1$ fixed (tentatively), the other coupling constants were finely adjusted to the fixed point [Eq. (2)] of an approximate real-space renormalization group (decimation). (In the renormalization-group context, the irrelevant operators are almost eliminated.) Second, with Γ regarded as a variable parameter, the location of the critical point $\Gamma = 1.0007(17)$ was determined through the finite-size-scaling analysis (of the energy gap). As mentioned above, right at the point (2), corrections to scaling are suppressed; in the lattice-field theory, such a lattice artifact is an obstacle to take the continuum limit reliably, and the idea, the so-called perfect action, has been developed for decades [16, 17, 18, 19].

The phase diagram of the model (1) is presented in Fig. 1. Here, the coupling constants other than D and H are set to Eq. (2). The D term is

reminiscent of the ϕ^4 -field-theory's mass term, $m^2\phi^2$, and the ferromagnetic (paramagnetic) phase appears for $D < (>)D_c = -0.39781956122$ (D_c : critical point) as anticipated. The magnetic field is set to $H = 0$ except in Sec. 2.4, where the H -stabilized two-magnon bound state is surveyed.

The rest of this paper is organized as follows. In Sec. 2, we present the simulation results, following an explanation of the technical preliminaries. In Sec 3, we address the summary and discussions.

2. Numerical results

In this section, we present the numerical results for the two-dimensional transverse-field Ising model, Eq. (1). We employed the numerical diagonalization method for the finite-size cluster with $N \leq 20$ spins. We implemented the screw-boundary condition (Novotny's method) [20] to treat a variety of system sizes $N = 8, 10, \dots, 20$ systematically; note that conventionally, the number of spins is restricted within the quadratic numbers, $N = 4, 9, \dots$, for a rectangular cluster. Here, we adopt the simulation algorithm presented in the Appendix of Ref. [14]. The linear dimension L of the cluster is given by

$$L = \sqrt{N}, \quad (3)$$

because N spins constitute a rectangular cluster.

2.1. Preliminaries: Character of the low-lying excitation levels

In this section, we explain the technical details, placing an emphasis on the character of the low-lying spectrum; see Fig. 2. As mentioned in Sec. 1, we employed the numerical diagonalization method for the quantum Ising model (1). The diagonalization was performed within the zero-momentum space, $k = 0$ (zone center), at which the one- and two-magnon excitation gaps, m_1 and m_2 , respectively, open. Hence, from the low-lying levels, $E_0 < E_1 < \dots$, at $k = 0$, we are able to calculate the mass gap of each excitation. As presented in Fig. 2, the character of the low-lying excitation depends significantly on either (a) $H = 0$ or (b) $H \neq 0$. For $H = 0$, because of the quasi-degeneracy of the ground states, the mass gaps $m_{1,2}$ are given by the formulas

$$m_1 = E_2 - E_0, m_2 = E_3 - E_0. \quad (4)$$

On the contrary, for $H \neq 0$, the quasi-degeneracy becomes resolved, and the relations

$$m_1 = E_1 - E_0, m_2 = E_2 - E_0, \quad (5)$$

hold. It is an advantage of the numerical diagonalization method that the low-lying levels are accessible directly.

Last, we address a technical remark. At $H = 0$, the Hamiltonian (1) restores the spin-inversion symmetry, $S_i^z \rightarrow -S_i^z$, and the parity index characterizes the levels $E_{0,1,2,3}$; that is, the levels $E_{0,2}$ ($E_{1,3}$) belong to the parity-even (odd) sector. Practically, the reduction of the Hilbert space with respect to the parity index saves the computational effort, because the evaluation of the fourth-lowest energy level E_3 is computationally demanding, and even unstable.

2.2. Finite-size-scaling analysis of m_2/m_1 ($H = 0$)

In this section, we analyze the critical behavior of the mass-gap ratio m_2/m_1 , devoting ourselves to the subspace, $H = 0$; see the phase diagram, Fig. 1.

To begin with, we consider the finite-size-scaling formula (6), which sets a basis of our analysis. (Tentatively, we turn on H .) The finite-size-scaling theory insists that the mass-gap ratio is expressed by the formula

$$m_2/m_1 = f((D - D_c)L^{1/\nu}, HL^{y_h}), \quad (6)$$

with a certain scaling function f , provided that the quantity m_2/m_1 is dimensionless (scale invariant) at the critical point; the scale invariance is confirmed by the simulation result presented below. The scaling parameters are set to the values appearing in the literatures, $(\nu, y_h) = [0.63002(10), 2.481865(50)]$ [15] and $D_c = -0.39781956122$ [14]. Hence, there is no adjustable parameter (arbitrariness) in the present scaling analyses.

Based on the above scaling formula (6), we turn to the analysis of the simulation result. In Fig. 3, we present the finite-size-scaling plot, $(D - D_c)L^{1/\nu} - m_2/m_1$, for various D , $N = 8, 10, \dots, 20$ and the fixed $H = 0$; the other coupling constants are fixed to Eq. (2). The data appear to collapse into a scaling curve satisfactorily; that is, the available system sizes already enter the scaling regime. Moreover, we confirm that the quantity m_2/m_1 is indeed scale-invariant (dimensionless) at the critical point $D - D_c = 0$. Actually, the mass-gap ratio appears to be around $m_2/m_1 \approx 1.8$ in good agreement with the preceding estimates (see the Introduction). In the next section, we estimate m_2/m_1 at the critical point, taking the extrapolation to the thermodynamic limit.

2.3. The mass-gap ratio m_2/m_1 at the critical point

In this section, we estimate the mass-gap ratio m_2/m_1 at the critical point, Eq. (2). In Fig. 4, we plot m_2/m_1 for $1/L^2$ [$N(=L^2) = 8, 10, \dots, 20$] at the critical point, Eq. (2). The least-squares fit to the data yields an estimate $m_2/m_1 = 1.83861(62)$ in the thermodynamic limit. As a reference, we made a similar least-squares-fit analysis for $14 \leq N \leq 18$, and arrived at a slightly enhanced estimate, $m_2/m_1 = 1.84311(92)$. The discrepancy $\Delta(m_2/m_1) \approx 0.005$ appears to dominate the least-squares-fit error ≈ 0.0006 . As a matter of fact, the data alignment in Fig. 4 exhibits a slight undulation, whose nodes locate around the system sizes of $N(=L^2) \approx 9, 16$ (quadratic numbers). Such an undulation is an artifact of the screw-boundary condition [20]; actually, there appears a slight hollow around $1/L^2 \approx 0.07 \sim 1/3.5^2$ (similarly, a bump around $1/L^2 \approx 0.05 \sim 1/4.5^2$). The above-mentioned discrepancy ≈ 0.005 causes a systematic error, which is not appreciated properly by the least-square-fit error. The discrepancy seems to be bounded by, at most, $1 \cdot 10^{-2}$. Hence, we estimate the mass-gap ratio as

$$m_2/m_1 = 1.84(1). \quad (7)$$

The estimate is examined by an independent analysis of m_2/m_1 ($H \neq 0$) in the next section.

We address a number of remarks. First, we argue the validity of the $1/L^2$ -extrapolation scheme, namely, the abscissa scale $1/L^2$ in Fig. 4. In Ref. [14], it was demonstrated that the $1/L^2$ -extrapolation scheme works successfully for the analysis of the critical indices of the model concerned, Eq. (1); the results turned out to be in good agreement with the existing values. Last, we make a comparison with the preceding transfer-matrix result $m_2/m_1 = 1.84(3)$ [11] for $N \leq 15$. The distance between the extrapolated value $m_2/m_1|_{N \rightarrow \infty} = 1.84$ and the raw $N = 15$ result $m_2/m_1|_{N=15} \approx 1.81$ is around $\Delta(m_2/m_1) = m_2/m_1|_{N \rightarrow \infty} - m_2/m_1|_{N=15} \approx 0.03$. On the one hand, the present data attain an improved convergence $\Delta(m_2/m_1) = m_2/m_1|_{N \rightarrow \infty} - m_2/m_1|_{N=20} \approx 0.017$. Clearly, the convergence of the raw data itself is improved possibly because of the expansion of the tractable system size, and the extension of the spin magnitude to $S = 1$.

2.4. Finite-size-scaling analysis of m_2/m_1 ($H \neq 0$)

In this section, we analyze the critical behavior of m_2/m_1 , applying a properly scaled magnetic field

$$H = A/L^{y_h}, \quad (8)$$

with the scaling dimension of the magnetic field, $y_h = 2.481865$ [15], and a coefficient

$$A = 11. \tag{9}$$

Afterward, we address a remark on the choice of A . We stress that the scaled magnetic field $H = A/L^{y_h}$ vanishes in the thermodynamic limit $L \rightarrow \infty$. In the experiment [13], such an infinitesimal magnetic field, the so-called effective longitudinal mean field [21], was induced (applied) so as to observe the two-magnon bound state beside the critical point clearly.

In Fig. 5, we present the finite-size-scaling plot, $(D - D_c)L^{1/\nu} - m_2/m_1$, for various D , $N = 8, 10, \dots, 20$, and the scaled magnetic field $HL^{y_h} = 11$, Eq. (8). The other scaling parameters and coupling constants (except D and H) are the same as those of Fig. 3. The data collapse into a scaling curve, supporting the validity of the scaling relation (6); in other words, the available system sizes already enter the scaling regime. Notably enough, in Fig. 5, there appears a plateau with the height $m_2/m_1 \approx 1.84$ extending in the symmetry-broken phase, $D - D_c < 0$. Moreover, the plateau width expands gradually, as the system size enlarges. Such a feature indicates an existence of a two-magnon bound state with $m_2/m_1 \approx 1.84$ for a wide range of the parameter space. The observation $m_2/m_1 = 1.84$ supports the estimate (7) obtained in Sec. 2.3.

A number of remarks are in order. First, we explain the choice of the coefficient $A = 11$ (9). The coefficient $A = 11$ was set so as to make the plateau in Fig. 5 flat. Specifically, the plateau slope becomes positive (negative) for $A > (<)11$. Second, it is to be noted that the plateau height $m_2/m_1 = 1.84$ is insensitive to the choice of the scaling parameters such as D_c and ν ; these parameters simply influence the horizontal drift of the plateau, leaving the plateau height unchanged. In this sense, the finite-size-scaling analysis under $H \neq 0$ provides unbiased information as to $m_2/m_1 \approx 1.84$. Last, it has to be mentioned that in the experiment [13], the mass-gap ratio was observed under a uniform magnetic field (effective longitudinal mean field [21]). In the experiment, the plateau height m_2/m_1 is directly observable without carrying out the scaling analysis, because the system size N of the sample material is sufficiently large.

3. Summary and discussions

The critical behavior of the two-magnon mass gap $m_2 (< 2m_1)$ (m_1 : one-magnon mass gap) was investigated for the two-dimensional spin- $S = 1$

transverse-field Ising model (1) by means of the numerical diagonalization method; the low-lying spectrum is directly accessible with the numerical diagonalization method, as presented in Fig. 2. The universal critical behavior of the mass-gap ratio m_2/m_1 is our concern. The spin- $S = 1$ model (1) allows us to incorporate a variety of interactions, which are adjusted to Eq. (2) so as to suppress [14] corrections to scaling. As a result, we estimate the mass-gap ratio as $m_2/m_1 = 1.84(1)$, Eq. (7). Our result is comparable with the preceding studies such as the Monte Carlo result $m_2/m_1 = 1.83(3)$ for a cluster up to $60^2 \cdot 120$ sites [4], the ϕ^4 -field-theoretical perturbative result $m_2/m_1 = 1.828(3)$ [10], the transfer-matrix-diagonalization result $m_2/m_1 = 1.84(3)$ for $N \leq 15$ [11], and the series-expansion result $m_2/m_1 \approx 1.81$ [12].

It is not very clear whether a bound state exists other than m_2 [4, 8]; it is likely that either the particles with m_1 and m_2 form a bound state with $m_3 (< m_1 + m_2)$ or a pair of particles m_1 constitute a series of excited states $m_{3,4,\dots}$. The continuum extending above $2m_1$ prohibits us from identifying a single-particle-excitation branch out of the continuum as in Fig. 2. As a matter of fact, for the one-dimensional quantum Ising model, there appear eight types of the magnon bound states with characteristic mass gaps, $m_1 < m_2 < \dots < m_8$ [3], and five branches are above the continuum threshold, $m_{4,5,\dots,8} > 2m_1$. It is suspected that the spectral function $f(\omega) = \langle 0 | S^-(\omega - \mathcal{H} + E_0)^{-1} S^+ | 0 \rangle$ with the ground-state vector $|0\rangle$ and the magnon-creation (annihilation) operator $S^{+(-)} = N^{-1} \sum_{i=1}^N S_i^{+(-)}$ detects a signal in the background (continuum). This problem is addressed in future study.

Acknowledgement

This work was supported by a Grant-in-Aid from Monbu-Kagakusho, Japan (Contact No. 25400402).

References

- [1] A.B. Zamolodchikov, Int. J. Mod. Phys. A **3** (1988) 743.
- [2] P. Fonseca and A. Zamolodchikov, J. Stat. Phys. **110** (2003) 527.
- [3] G. Delfino, J. Phys. A **37** (2004) R45.
- [4] M. Caselle, M. Hasenbusch, and P. Provero, Nucl. Phys. B **556** (1999) 575.

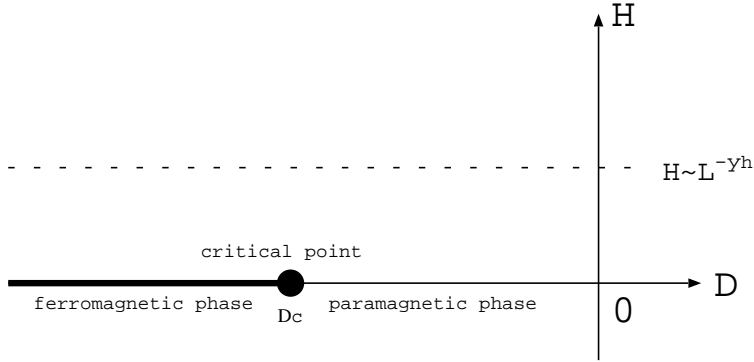


Figure 1: The phase diagram of the two-dimensional spin- $S = 1$ transverse-field Ising model (1) for the single-ion anisotropy D and uniform magnetic field H is presented. [The other coupling constants are fixed to Eq. (2).] The solid line denotes the first-order phase boundary, and at the endpoint, $(D, H) = (D_c, 0)$, the critical point separating the paramagnetic and ferromagnetic phases locates. The two-magnon bound state (Fig. 2) in the vicinity of the critical point is our concern. The subspace of $H \propto L^{-y_h}$ (dashed line) is surveyed in Sec. 2.4.

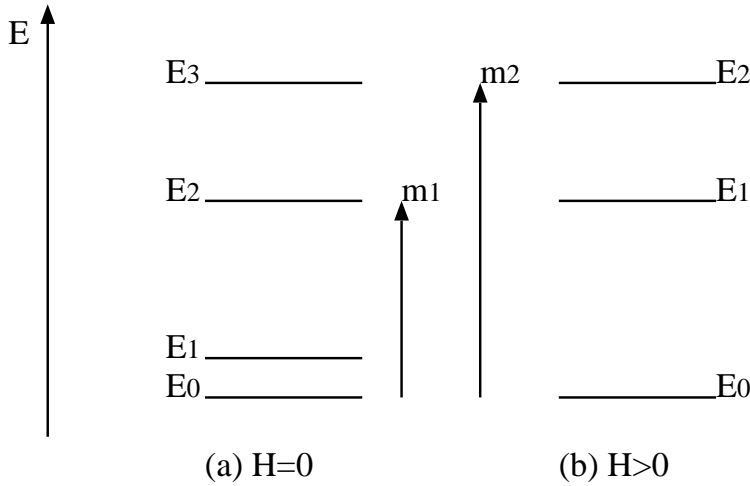


Figure 2: A schematic drawing of the low-lying excitation levels, $E_0 < E_1 < \dots$, for the transverse-field Ising model (1) in the vicinity of the critical point is presented. Here, the zero-momentum subspace $k = 0$ is considered; at $k = 0$, the one- and two-magnon excitation gaps, m_1 and m_2 , respectively, open. The spectral structure depends on (a) $H = 0$, and (b) $H > 0$ significantly.

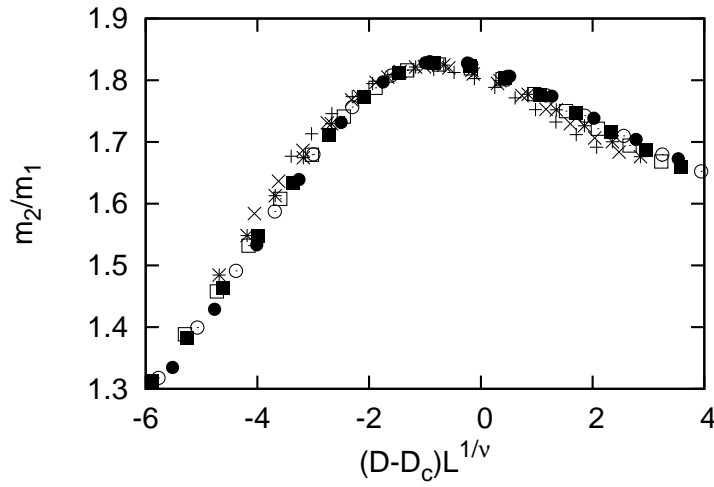


Figure 3: The finite-size-scaling plot, $(D - D_c)L^{1/\nu} - m_2/m_1$, for various D , $N = 8, 10, \dots, 20$, and the fixed magnetic field $H = 0$ is shown; the symbols, $+$, \times , $*$, \square , \blacksquare , \circ , and \bullet , denote the system sizes $N = 8, 10, 12, 14, 16, 18$, and 20 , respectively. Here, the scaling parameters are set to the values appearing in the literatures, $\nu = 0.63002$ [15] and $D_c = -0.39781956122$ [14]. [The coupling constants (except D) are set to Eq. (2).] The mass-gap ratio m_2/m_1 appears to take a scale-invariant value at the critical point $D - D_c = 0$, and the precise value is estimated in Fig. 4.

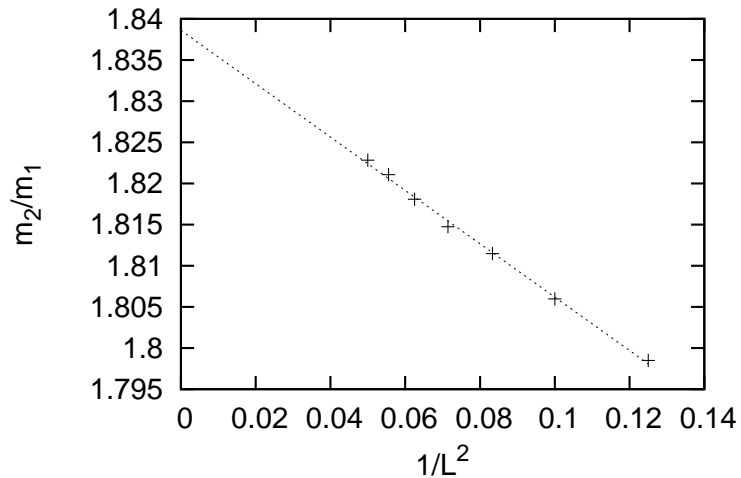


Figure 4: The mass-gap ratio m_2/m_1 at the critical point, Eq. (2), is plotted for $1/L^2$ [$N(= L^2) = 8, 10, \dots, 20$]; The least-squares fit to these data (dotted line) yields an estimate $m_2/m_1 = 1.83861(62)$ in the thermodynamic limit. The series of data exhibit a slight undulation due to the screw-boundary condition [20]. A possible extrapolation (systematic) error is considered in the text.

- [5] V. Agostini, G. Carlino, M. Caselle, and M. Hasenbusch, Nucl. Phys. B **484** (1997) 331.
- [6] P. Provero, Phys. Rev. E **57** (1998) 3861.
- [7] M. Caselle, M. Hasenbusch, P. Provero, K. Zarembo, Phys. Rev. D **62** (2000) 017901.
- [8] R. Fiore, A. Papa, and P. Provero, Phys. Rev. D **67** (2003) 114508.
- [9] D. Lee, N. Salwen, and M. Windolowski, Phys. Lett. B **502** (2001) 329.
- [10] M. Caselle, M. Hasenbusch, P. Provero, and K. Zarembo, Nucl. Phys. B **623** (2002) 474.
- [11] Y. Nishiyama, Phys. Rev. E **77** (2008) 051112.
- [12] S. Dusuel, M. Kamfor, K. P. Schmidt, R. Thomale, and J. Vidal, Phys. Rev. B **81** (2010) 064412.

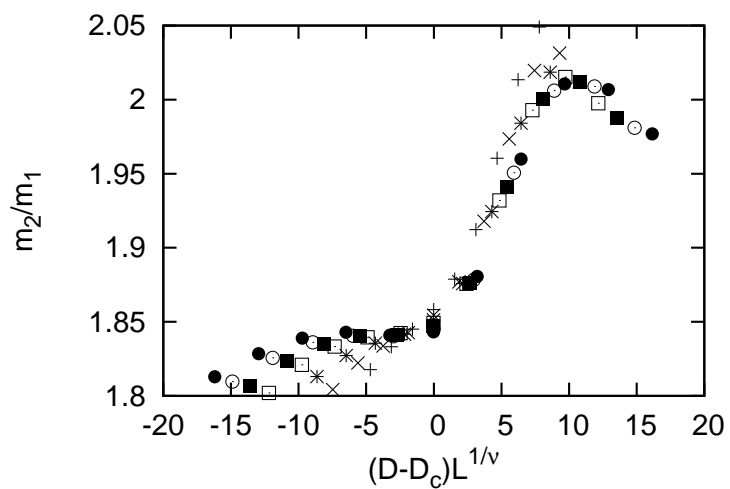


Figure 5: The finite-size-scaling plot, $(D - D_c)L^{1/\nu} - m_2/m_1$, for various D , $N = 8, 10, \dots, 20$, and scaled magnetic field, $H = 11/L^{y_h}$ ($y_h = 2.481865$ [15]) is shown; the symbols, $+$, \times , $*$, \square , \blacksquare , \circ , and \bullet , denote the system sizes $N = 8, 10, 12, 14, 16, 18$, and 20 , respectively. Here, the scaling parameters and the coupling constants (except D and H) are the same as those of Fig. 3. A plateau develops in the ferromagnetic phase ($D < D_c$), indicating an existence of a H -stabilized bound state for a finite range of D . The plateau height $m_2/m_1 \approx 1.84$ supports the estimate, Eq. (7).

- [13] R. Coldea, D. A. Tennant, E. M. Wheeler, E. Wawrzynska, D. Prabhakaran, M. Telling, K. Habicht, P. Smeibidl, and K. Kiefer, *Science* **327** (2010) 177.
- [14] Y. Nishiyama, *Nucl. Phys. B* **832** (2010) 605.
- [15] M. Hasenbusch, *Phys. Rev. B* **82** (2010) 174433.
- [16] K. Symanzik, *Nucl. Phys. B* **226** (1983) 187.
- [17] K. Symanzik, *Nucl. Phys. B* **226** (1983) 205.
- [18] H.G. Ballesteros, L.A. Fernández, V. Martín-Mayor, and A. Muñoz Sudupe, *Phys. Lett. B* **441** (1998) 330.
- [19] M. Hasenbusch, K. Pinn, and S. Vinti, *Phys. Rev. B* **59** (1999) 11471.
- [20] M.A. Novotny, *J. Appl. Phys.* **67** (1990) 5448.
- [21] S. T. Carr and A. M. Tsvelik, *Phys. Rev. Lett.* **90** (2003) 177206.